Thermal interactions of the AD79 Vesuvius pyroclastic density currents and their deposits at Villa dei Papiri (Herculaneum archeological site, Italy)

Giordano G.*[1], Zanella E.[2], Trolese M.[1], Baffioni C.[1], Vona A.[1], Caricchi C.[3], De Benedetti A.A.[1], Corrado S.[1], Romano C.[1], Sulpizio R.[4], Geshi N. [5]

[1] Università Roma Tre, Largo San Leonardo Murialdo 1, 00146, Roma, Italia

[2] Università di Torino, Via Valperga Caluso 35, 10125 Torino, Italy

[3] Istituto Nazionale di Geofisica e Vulcanologia, Via Vigna Murata 605, 00143 Roma, Italia

[4] Università di Bari, Via Edoardo Orabona, 4, 70126 Bari

[5] Geological Survey of Japan, AIST Site 7, 1-1-1 Higashi, Tsukuba, Ibaraki 305-8567, Japan

*corresponding author: email guido.giordano@uniroma3.it

Abstract. Pyroclastic density currents (PDCs) can have devastating impacts on urban settlements, due to their dynamic pressure and high temperatures. Our degree of understanding of the interplay between these hot currents and the affected infrastructures is thus fundamental not only to implement our strategies for risk reduction, but also to better understand PDC dynamics. We studied the temperature of emplacement of PDC deposits that destroyed and buried the Villa dei Papiri, an aristocratic Roman edifice located just outside the Herculaneum city, during the AD79 plinian eruption of Mt Vesuvius (Italy) by using the thermal remanent magnetization of embedded lithic clasts. The PDC deposits around and inside the Villa show substantial internal thermal disequilibrium. In areas affected by convective mixing with surface water or with collapsed walls, temperatures average at around 270°C (min 190°C, max 300°C). Where the deposits show no evidence of mixing with external material, the temperature is much higher,

averaging at 350°C (min 300°C; max 440°C). Numerical simulations and comparison with temperatures retrieved at the very same sites from the reflectance of charcoal fragments indicate that such thermal disequilibrium can be maintained inside the PDC deposit for time-scales well over 24 hours, i.e. the acquisition time of deposit temperatures for common proxies. We reconstructed in detail the history of the progressive destruction and burial of Villa dei Papiri and infer that the rather homogeneous highest deposit temperatures (average 350°C) were carried by the ash-sized fraction in thermal equilibrium with the fluid phase of the incoming PDCs. These temperatures can be lowered on short time- (less than hours) and length-scales (meters to tens of meters) only where convective mixing with external materials or fluids occurs. By contrast, where the Villa walls remained standing the thermal exchange was only conductive and very slow, i.e. negligible at 50 cm distance from contact after 24 hours. We then argue that the state of conservation of materials buried by PDC deposits largely depends on the style of the thermal interactions. Here we also suggest that PDC deposit temperatures are excellent proxies for the temperatures of basal parts of PDCs close to their depositional boundary layer. This general conclusion stresses the importance of mapping of deposit temperatures for the understanding of thermal processes associated with PDC flow dynamics and during their interaction with the affected environment.

1. Introduction

The main impact factors of pyroclastic density currents (PDCs) within their inundation areas are their temperature and dynamic pressure. While dynamic pressure is quantitatively related to the local momentum of the current (i.e. the instantaneous mass discharge over a certain area, e.g. a building; Dioguardi & Dellino, 2014), factors affecting

54 the local temperature are much less understood. The general understanding is that, given
55 an initial temperature of the pyroclastic mixture at vent (which largely depends on magma
56 composition, possible interaction with ground- or surface-water, and amount of cold lithics
57 excavated), the mass flux fundamentally controls the thermal energy dissipation within
58 PDCs (Doronzo et al., 2016; Giordano and Doronzo, 2017; Trolese et al., 2017), along with
59 the entrainment of cold materials such as accidental lithics, vegetation, surface water and
60 snow (e.g. Paterson et al., 2010). The available datasets for temperature of pyroclastic
61 flow deposits either directly measured or retrieved from various methods (Table S1 in
62 Appendix 1) indicate that temperatures may vary substantially and almost irrespectively of
63 the PDC size, chemistry, lithic content, and lithofacies (e.g. Cioni et al., 2004; Zanella et
64 al., 2015; Pensa et al., 2015a, Trolese et al., 2017). For example, ash clouds associated
65 with confined PDCs have been observed to leave behind thin and cold veneer deposits at
66 Tungurahua volcano in 2006 (Eychenne et al., 2012) while similar occurrences were able
67 to burn houses at Montserrat in 1997 and Merapi in 2010 (e.g. Jenkins et al., 2013).
68 Similarly, thick valley pond ignimbrite deposits are known to vary from completely and
69 laterally extensively welded (e.g. Willcock et al., 2013; Lavallée et al., 2015) to unwelded,
70 with T ranging from > 600°C (e.g. Lesti et al., 2011, Trolese et al., 2017) to low
71 temperatures close to detection limits of common methods (e.g. McClelland et al., 2004).
72 Given these uncertainties, much debate has fuelled the literature on defining the actual
73 significance of temperature proxies measured in the deposits (e.g. McClelland and Druitt,
74 1989; Cioni et al., 2004; Paterson et al., 2010; Sulpizio et al., 2008; 2015; Zanella et al.,
75 2015; Pensa et al., 2015a,b). The most used proxy is the thermal remanent magnetization
76 (TRM) of lithic clasts, and for example McClelland and Druitt (1989), Bardot (2000), Cioni
77 et al. (2004) and Zanella et al. (2007) made a distinction between the temperature of
78 pyroclastic flows and that of their deposits. Based on the longer time required for thermal
79 equilibration of lithics respect to their residence in the flow, TRM-derived T are commonly

interpreted as reflecting the deposit temperature rather than that of the parent flow. Even longer is the equilibration time for charcoalification of wood (Scott and Glasspool, 2005; Caricchi et al., 2014). Furthermore, by comparing the TRM on lithics and the degree of charcoalification of wood, Pensa et al. (2015a,b) warned us about the complicated history of pre-heating of lithic clast which may be extracted anywhere from deep in the conduit, from the vent, or picked up along flow, all potentially carrying very different temperatures at their final landing.

Other important though rather poorly explored topics are: i) what is the relative contribution to the final temperature at deposition of the polycomponent and polydispersed pyroclastic debris, and ii) how long it takes for the deposit to significantly depart from the temperature of the parent pyroclastic flow when compared with the characteristic time of thermal equilibration for the different proxies.

In this paper, we analyse in detail the temperature of the pyroclastic flow deposits of the AD79 eruption at Vesuvius. Unlike other previous work that approached the problem at the volcano scale (e.g., Cioni et al., 2004; Zanella et al., 2007, 2015), we work here to define the thermal interactions over time of one building progressively buried by hot PDC deposits. We use TRM analysis of lava lithic clasts sampled across stratigraphy and different lithofacies of the PDC deposits in and around the Roman Villa dei Papiri at Herculaneum, famous for the unique preservation of rare and delicate papyri documents (Guidobaldi et al., 2009; Mocella et al., 2015). The innovative contribution of our site-specific approach is to clarify the importance of fine-scale interactions of PDC deposits with the urban fabric, which determine significant local variations in temperature and cooling rates. Such variations may explain the variable thermal impact observed on infrastructures and other archeological remains in the Villa dei Papiri, as well as in the nearby city of Herculaneum and in other main cities affected by the AD79 eruption, e.g. Pompeii and Oplontis. Our field dataset and thermal numerical modeling indicate that the

morphological configuration of the contact between the hot PDC deposits and the cold edifice determines the time scale of the thermal exchange, promoting much faster cooling where debris derived from the partial collapse of the edifice mixed with the pumice and ash PDC deposits. Furthermore, we interpret the temperature of the PDC deposit derived from TRM as largely recording a disequilibrium temperature dominated by the ash fraction, which cannot be substantially different from that of the parent flow. Hence, with the exception of local effects associated with physical mixing with water or sediment or other external cold materials, such as collapsed wall debris, the deposit temperature closely reflects the flow dynamic processes that determine the extent of heat loss of the ash fraction prior to deposition.

2. Summary of the AD79 eruption and the deposits of Herculaneum excavations

The chronology of the AD79 eruption is based on the accounts of Pliny the Younger and translated to processes and timing by Sigurdsson et al. (1982, 1985). The stratigraphy has been divided into 8 Eruption Units by Cioni et al. (1992, 2004). The stratigraphy in Herculaneum is described in Gurioli et al. (2002).

The eruption started on August 24 at around noon with a not better specified phreatomagmatic event (EU1: phreatomagmatic ash). At around 1PM a buoyant column rose up to 30-33 km high (Carey and Sigurdsson, 1987) producing stratified SE-ward-dispersed fall deposits. The first pulse lasted till around 8PM (EU2f phonolitic white pumice lapilli) and the second across the night (EU3f phonotephritic grey pumice lapilli). During this early phase, partial collapses produced the pyroclastic flows (EU2/3pf and EU3pf) that reached Herculaneum (Barberi et al., 1989).

During the following day, on August 25, the onset of the caldera collapse eventually led to the generation of radially spreading pyroclastic flows (EU4-5-6-7; Cioni et al., 2004; Gurioli

et al., 2007), with lithic rich breccias (EU6) and evidence for magma-water interaction (Barberi et al., 1989; Cioni et al., 1992). The eruption ended with the deposition of a thick, phreatomagmatic, accretionary lapilli-bearing ash (EU8).

According to the stratigraphy in Gurioli et al. (2002) and Caricchi et al. (2014), Herculaneum did not receive the deposition of the initial pumice fallout, being cross-wind respect to dispersal axis. The stratigraphic succession records the PDC deposits (E2/3pf; EU3pf) associated with the partial collapses of the column during the transition between phonolitic EU2 and phonotephritic EU3 phases, and later PDC deposits of the caldera forming phase (EU4 to EU8).

3. Previous work, materials and methods

The stratigraphy and sedimentology of the AD79 Vesuvius eruption deposits have been studied in detail in several works (e.g. Lirer et al., 1973; Sigurdsson et al., 1982, 1985; Carey and Sigurdsson, 1987; Cioni et al.,1992; Yokoyama and Marturano,1997; Gurioli et al., 2002, 2005). The temperature of emplacement of the PDC deposits has been investigated with various methods, including TRM on lithic clasts (Kent et al., 1981; Cioni et al., 2004; Gurioli et al., 2005; Zanella et al., 2007; 2015), bone fragment analysis (Mastrolorenzo et al., 2001), and charcoal fragments (Caricchi et al., 2014). The inferred deposit temperatures retrieved from the various proxies range from 100°C to 500°C, with most common values around 250-370°C (see Appendix 1). These data represent an excellent benchmark to our study, as they provide the overall thermal framework for the AD79 PDC deposits, which allows us to go into the detail of the PDC thermal impact at the individual building scale, something that has never been previously attempted. We selected as case study the aristocratic Roman Villa dei Papiri, which was located just outside the main Herculaneum city (Fig. 1a,b), along the AD79 coastline (Guidobaldi et al.,

159 2009). The Villa was reached by the early intra-plinian PDC and progressively buried and
160 partially destroyed by the following PDCs that deposited more than 30 m of dominantly
161 massive lapilli tuff (Fig. 1c,d).
162 The temperature of the PDC deposits that buried and destroyed the Villa dei Papiri was
163 retrieved from the determination of the TRM of the lithic clasts sampled in the lapilli tuff of
164 units EU2/3pf, EU3pf, EU4 (Fig. 1c,d). Details on the TRM method are given in Appendix
165 1. Eight sites (VP1, VP2, VP5.1-3-5-7-10, VP9) were sampled where the ash matrix <
166 1mm represents > 75% of the deposit (see Appendix 2). In particular, the transect VP5.1-
167 3-5-7-10 has been devised to reconstruct the extent of the thermal interaction between the
168 standing perimeter wall of the Villa and the PDC deposits.
169 Additional four sites were sampled in order to identify the role of different sources of
170 thermal interaction with the PDC deposits. To this aim we sampled: (a) a fines-depleted
171 facies within a large gas-pipe (VP8); (b) a strongly zeolitised facies likely associated with
172 the influence of external water during cooling (VP6); and (c) a chaotic breccia facies made
173 of mixed coarse debris from the partial collapse of the Villa walls and the PDC deposit
174 (VP3, VP4).
175 Four out of our twelve sampling sites (i.e. VP1, VP2, VP3, VP4) correspond to the very
176 same sites where emplacement temperatures had been previously interpreted from
177 charcoal fragments in Caricchi et al. (2014). We devised this sampling strategy in order to
178 first compare the TRM data with those retrieved from an independent proxy. This is
179 because previous work has pointed out that, while TRM is a very powerful method for the
180 estimation of the temperature of PDC deposits, the thermal history of each sampled clast
181 may vary and induce some uncertainties on the results (e.g. Pensa et al., 2015a).
182 This approach allowed us to extend with high degree of confidence the use of TRM of
183 lithics in the desired sites around the Villa, where charcoal fragments are not available.
184 In addition, charcoal equilibrates with the embedding deposits in timescales of 10^1 hours,

usually 24 hours or more (Scott and Glasspool, 2005; Caricchi et al., 2014), while cm-sized lithics do so within much shorter timescales, usually < 10^0 hours (Bardot, 2000; Cioni et al., 2004). By comparing TRM data and published charcoal data from the very same sites, we aim therefore also at appreciating the influence of thermal disequilibrium processes, such as those associated with the time-scale of cooling of the deposit.

We sampled lithics in the size range of about 1-3 cm, but mostly around 1 cm, taken from massive and chaotic facies (Appendix 2). Samples are all unaltered lava clasts deriving from the shallow cone of Vesuvius volcano, in order to minimize the complexity related to their magnetic mineralogy and thermal history (e.g. Cioni et al., 2004; Pensa et al., 2015a). The small diameter of the sampled lithics allows us to be sure of their thermal equilibrium with the embedding deposits (Bardot, 2000). On the other hand, it makes it difficult to accurately orient them in the unconsolidated PDC deposits, which we take as an acceptable limitation, giving that previous studies have already shown that the deposits have a low temperature component (Cioni et al., 2004; Zanella et al., 2007; see also more detailed explanation in Appendix 1).

INSERT FIG. 1 HERE

4. Results

4.1 Thermal remanent magnetization of lithic clasts

The temperature of PDC deposits is usually retrieved from the principal components of magnetization, in the form of progressive thermal demagnetization data, of the embedded lava clasts (e.g. McClelland and Druitt, 1989; Porreca et al., 2006). This procedure is aimed at reproducing the natural event of a lava fragment eroded from the

conduit/vent/volcano-slope and eventually incorporated in a PDC deposit. For PDC deposit temperatures below the Curie temperature of magnetic minerals present in the lava clast (or the maximum value of the blocking temperatures [T_b] spectrum), the clast will show two magnetization components during progressive thermal demagnetization, characterized by different directions of their magnetic vector. These two magnetic directions represent respectively: i) the low-T component acquired by the lava clast within the PDC deposit during cooling from the temperature of emplacement to ambient; ii) the high-T component acquired by the lava clasts prior to its incorporation within the PDC, randomized by the chaotic transport and depositional processes. Thus, during the progressive demagnetization of the sample in the lab, the re-heating temperature (T_r) is determined to be between the highest T_b at which the low-T component is fully removed and the next temperature step, which is where the original magnetization starts to be thermally demagnetized, until the Curie temperature.

The analysis of the Zijderveld diagrams (Fig. 2) provides the magnetization components and the T_r interval. The analysis of the demagnetization paths of the 190 measured specimens allowed to determine well defined T_r intervals for the majority of lithic samples (72%) (Table 1). According to the classification proposed by Cioni et al. (2004; details are given in Appendix 1), paths with sharp change in direction of the magnetic vector are of "type C" and their T_r intervals are determined in a range of 40 °C (Fig. 2a-k; Table 1). Clasts that during demagnetization changed the direction of the magnetic vector across a curvilinear interval are classified as "type D" (Fig. 2l; Table 1). In this case, their T_r interval is wider, normally more than 80 °C. The remaining 9% of analysed clasts showed a single component of magnetization. These correspond to types A and B of Cioni et al. (2004) and without orientation cannot be resolved (Table 1; Fig. S1 in Supplementary material). Another 19% of clasts are characterized by the angle between the two magnetization components <15° so that we do not use them confidently for the determination of T_r (cf.

237 Porreca, 2004).

238 Samples from site VP1 yield natural remanent magnetization (NRM) intensities that vary
239 from 2 x 10^{-3} to 1.34 A m^{-1}, and their magnetization was fully unblocked at temperature
240 between 420°C and 520°C. In most of the cases (type C and D; about 62%) the low-T
241 component is removed at 180 – 480°C. All but one sample at site VP2 have two distinct
242 components of magnetization (type C and D, about 94%), with NRM intensity ranging from
243 1.4 x 10^{-2} to 2.88 A m^{-1}. The high-T component persists up to a temperature of about
244 560°C, while the remanence of the low-T component is unblocked between 200°C and
245 400°C. The NRM intensity of lithic clasts from site VP3 varies between 2 x 10^{-3} and 1.42 A
246 m^{-1}, which decreases until the samples are fully demagnetized by 420 – 560°C. Most of
247 the samples belongs to type C and D (about 66%), with the low-T component that is
248 removed at temperature intervals ranging from 200°C to 340°C. Lithic clasts from site VP4
249 are completely demagnetized between 480°C and 520°C, and their NRM intensity ranges
250 from 10^{-3} to 1.56 A m^{-1}. The temperature interval at which the low-T component of type C
251 and D samples (about 63%) is isolated varies between 220°C and 320°C. The remanence
252 of samples from sites VP5-1, 3, 5, 7 and 10 is stable up to temperatures between 440°C
253 and 560°C. The NRM intensities vary from 3 x 10^{-3} to 3.36 A m^{-1}. Most lithic clasts behave
254 as type C and D (about 75%), and their low-T component is unblocked over a temperature
255 range from about 200°C to 440°C. Almost all lithic clasts collected from site VP6 (about
256 82%) have two distinct magnetic vectors, and their NRM intensity ranges from 2.6 x 10^{-1} to
257 3.18 A m^{-1}. The low-T component is removed at demagnetization between 220°C and
258 360°C, whereas the high-T component persists until treatment at 540°C. All the lithic clasts
259 from site VP8 show three magnetization components, whose layout highlights two T_r
260 intervals: one in the range 280-320 °C, the other in the range 180-200 °C. The former is
261 fully consistent with the T_r intervals determined in all the other sampling sites; the latter
262 represents the lowest T_r intervals within Villa dei Papiri. The magnetization of these

samples is completely removed between 400°C and 560°C, with NRM intensities ranging from 7 x 10^{-3} to 2.53 A m^{-1}. Lithic clasts from site VP9 are completely thermally unblocked by 520 – 620°C, with NRM intensities that range from 4.8 x 10^{-2} to 1.11 A m^{-1}. Half of these samples exhibits two magnetic components (type C and D, 50%), which are separated by a change in direction around 240 – 480°C.

INSERT FIG 2 HERE

According to the procedure adopted by Cioni et al. (2004) and Zanella et al. (2007, 2014), we determined the mean deposit temperature (T_{dep}) of each sampling site as the range where the greatest number of T_r intervals falls (Fig. 3). This method has its main limit in the qualitative approach. Nevertheless, the fact that both the studied deposits and the lithic fragments are heterogeneous (no information is at priori available on the thermal history of the lava clasts and on their magnetic properties) reinforces the reliability of the results (Zanella et al., 2015). Besides, a statistical approach for T_{dep} estimation based on the Gaussian method has been recently applied to the Minoan eruptive deposits of Santorini (Tema et al., 2015). Results obtained from the mathematical method were fully consistent with those from the overlapping method. T_{dep} intervals are listed in Table 1. The T_{dep} varies from 180 to 440 °C with mean values ranging from 280-340 °C (Table 1). This range is fully consistent with the T_{dep} values already reported for the AD79 deposits around Vesuvius (Cioni et al., 2004). The lowest interval is displayed in VP8, whose lithic clasts have been sampled in a gas-pipe.

INSERT FIG. 3 AND TABLE 1 HERE

4.2 Interpretation of TRM data

290 TRM data at Villa dei Papiri show quite a large variability ranging from 180°C to 440°C.
291 These data are consistent with previously published data on deposit temperature obtained
292 from charcoal fragments at some of the very same localities (Fig. 1; Table 1; cf. Caricchi et
293 al., 2014). We therefore trust that all our temperature estimates are accurate (cf. Pensa et
294 al., 2015b), although they need to be addressed for their variations in such a very limited
295 area. These variations partly reflect the stratigraphy, where the three sites sampled in the
296 lower unit EU2/3pf (VP4, VP6 and VP8) show the lowest T_{dep} values (Fig. 1 and Table 1).
297 In particular, site VP8, with a T_{dep} of 180-200°C, was sampled within a large gas pipe
298 generated by the interaction of the incoming PDC with the sea shoreline (Fig. 4b and
299 Appendix 2). The presence of two LT components in the site VP8, with the intermediate
300 one consistent with deposit temperatures away from the pipe, can be explained by the
301 time lag required for the gas pipe to form: initially the clasts equilibrated part of their
302 magnetization within the hot PDC deposit and later rotated when the vapourised sea water
303 percolated through the deposit forming the gas pipe, allowing for the acquisition of a
304 secondary LT (e.g. Porreca et al., 2014). Lithic clasts of site VP6, with a T_{dep} of 280-320°C,
305 were collected within the zeolitised halo around the pipe (Fig. 1d and Appendix 2), also
306 likely generated by the upward percolation of vapourised seawater at the paleoshoreline.
307 Site VP4, with a T_{dep} of 260-300°C, was instead sampled in a breccia facies made of
308 mixed pyroclastic material and debris from collapsed wall of the Villa (Fig. 4c and Appendix
309 2). At this site VP4 the temperature from TRM of lithics is in perfect agreement with that
310 retrieved by Caricchi et al. (2014) from reflectance analysis of charcoal fragments
311 embedded in the very same site (Table 1). We interpret therefore the low values
312 associated with EU2/3pf as related to a significant interaction of the incoming PDCs with
313 the environment, either seawater or the partially destroyed Villa. Data from the upper units
314 EU3pf and EU4 (VP1, VP2, VP5.1-3-7-10) are on average much higher (Table 1) and
315 indicate temperatures that are consistent with maximum values reported in literature as

316 characteristic of the AD79 deposits outside towns (Cioni et al., 2004; Zanella et al., 2007;
317 2015). Noticeable exceptions are sites VP3 and VP5.5. Site VP3 is located inside the
318 building where the EU4 deposit is admixed with collapsed walls (Fig. 4d and Appendix 2).
319 Also for this site data from reflectance analysis of charcoal fragments embedded in the
320 very same site are available (Caricchi et al., 2014; Table 1) and match perfectly with our
321 TRM data. Therefore, like for VP4, we interpret the lower temperatures in terms of cooling
322 effect of the edifice debris. Site VP5.5 is instead somewhat problematic as it is far from the
323 edifice and closely surrounded by sites characterised by much higher temperatures. Its
324 lower average temperature may either be an outlier or indicate that the site was affected
325 by some cooling agent difficult to identify (e.g. a close gas pipe present in the third
326 dimension but invisible along the exposed face where lithics had been sampled; Fig. 1c).
327 In summary, the average of the mean values obtained for each of the sites affected by
328 evident cooling agents (VP4, VP6, VP8, VP3) gives a value of 272°C (Fig. 5). This
329 temperature contrasts with a similar average for sites unaffected by evident cooling agents
330 (VP1, VP2, VP5.1-3-5-7-10, VP9) where the value is 348°C (Fig. 5). It must be noticed that
331 sites VP1, VP2 and VP5.1 are located at distances of less than 1 m from the intact Villa
332 walls (Fig. 1c) and bear no edifice debris inside. This indicates that the presence of the
333 Villa edifice was “felt” by the deposit in terms of heat transfer generating thermal
334 disequilibrium at short time and length scales only where the collapsed walls physically
335 mixed with the pyroclastic material. Conversely, in absence of physical mixing with cold
336 debris, the pyroclastic deposit is very poorly affected by the temperature of the substrate.
337 Similarly, the convective mixing with seawater is an efficient cooling agent for the PDC
338 deposit.
339
340 INSERT FIG. 4 AND FIG. 5 HERE
341

5. Numerical Modeling

In order to better understand the time and length scales of the thermal interaction between PDC deposits and the Villa dei Papiri edifice, we performed numerical simulations of the burial of the Villa. The numerical code used is the open source HEAT3D (Wohletz et al., 1999; Wohletz, 2008). We computed only the conductive heat transfer between the hot PDC deposits and the wall of the Villa at ambient temperature, as convection in the deposit is negligible. Details on the numerical approach used to solve our specific case study are given in Appendix 3. We disregarded the effect of the preceding convective thermal interaction between the flowing PDC and the building, since the dataset we used derives from equilibration temperatures of lithics embedded in the deposit: we are consequently herein only interested in the thermal interactions between the PDC deposit and the building. Furthermore, this assumption is conservative as the transient thermal effect, if any, of the flowing PDC (duration of minutes) on the building could only be that of a limited pre-heating of the walls, in fact reducing their thermal disequilibrium with the PDC deposit. For modeling purposes, we defined a 3 m x 3 m computational domain with a 5 cm cell-grid. These dimensions are intended to represent the interior of the 40 m thick and laterally extensive PDC deposit that rapidly buried the Villa, so that we can disregard boundary effects such as the deposit-air and the deposit-underlying base interactions. Furthermore, the selected dimensions allow to balance the need for a fine cm-sized cell-grid that compares with the dimensions of the lithics analysed for TRM (see previous section) and optimise computational resources. The model integration time for this configuration is 15 minutes, which is much shorter than the acquisition time for both the charcoal and the lithic proxies, and therefore is perfectly suited to represent the full process of thermal exchange. We defined two configurations (Fig. 6): configuration A is aimed at simulating the thermal exchange between a vertical standing wall (1 m thick) of

368 the Villa and the PDC deposit, to a distance of 2 m from the wall (e.g. VP1, VP2, VP5-1);
369 configuration B is aimed at simulating the thermal exchange where the wall is collapsed
370 and broken in pieces embedded within the PDC deposit (e.g. VP3 and VP4). We
371 represented the collapsed portion as a 2 m thick horizontal layer where the average wall-
372 clast is a square 25 cm across, mixed at 50% with the PDC deposit, and covered by 1 m of
373 PDC deposit. A finer grain size with wall-clasts of 2.5 cm is considered in Appendix 3.
374 Considering that the selected dimensions of the computational domain are much smaller
375 compared to the full extent and thickness of the PDC deposit, the boundary conditions for
376 the PDC deposit in both configurations are assigned and fixed to 350°C, representing the
377 continuous ability of the PDC deposit around the domain to provide thermal energy.
378 However, we also tested the effect of cooling in air from the upper boundary of the deposit
379 (not shown), which resulted to be negligible over the 24 h of computation time at just 50
380 cm below surface. Table 2 shows the parameters used to characterise the building and the
381 deposit physical properties. We represented the PDC deposit as a continuum at the scale
382 of simulation, with a bulk density of 1200 kg m^{-3}. This value results by considering a 'dense
383 rock equivalent' density for phonolitic magma of 2400 kg m^{-3} (Lange and Carmichael,
384 1987) and a total deposit porosity of 50%, accounting both for the porosity of pumice and
385 intergranular voids. For selecting the appropriate value of thermal conductivity (k) of the
386 bulk PDC deposit, we considered that thermal conductivity scales linearly with porosity
387 (e.g. Robertson, 1988). We have therefore used the values provided in Whittington et al.
388 (2009) for volcanic glass at 1.4 W $m^{-1}K^{-1}$, which, for the given porosity of 50%, gives a
389 value of 0.7 W $m^{-1}K^{-1}$. Specific heat (Cp) is taken at 1200 J kg^{-1} K^{-1}, consistent with
390 literature data (e.g. Whittington et al., 2009). All values selected for our modeling and
391 shown in Table 2 are in agreement with average values for unconsolidated (porous) tuffs
392 and for walls made of bricks and cement (e.g. Turcotte and Schubert, 2014; Eppelbaum et
393 al., 2014). The initial T of the PDC deposit is taken at 350°C, that is the average of our

394 data away from the building (from transect VP5) and in agreement with previous
395 estimations (e.g. Zanella et al., 2007). The selection of constant k and Cp values during
396 the simulations is justified in the range of temperatures simulated (ambient – 350°C),
397 wherein P-T dependencies are negligible.
398
399 INSERT TABLE 2 HERE
400
401 Time steps of the numerical solutions are determined by the dimension of the cells so that
402 the minimum simulated is 15 minutes, lower than the time of acquisition of the TRM signal
403 by the analysed lithics. Runs simulated 24 hours of thermal exchange between the PDC
404 deposits and the Villa, which is longer than the time of acquisition for charcoal. We are
405 therefore able to analyse the temperature variations in the deposit in a time-frame that
406 encompasses the time-scales of acquisition for both TRM and charcoal proxies.
407 Results indicate that configuration A promotes very little heat transfer during the first 24
408 hours, with a T drop of less than 50°C in the deposit at 50 cm distance from the contact
409 with the wall and almost no variations at 1 m distance (Fig. 6c). This explains why the
410 temperatures acquired by both the lithic and the charcoal proxies at sites even close to the
411 Villa walls (e.g. VP2), but where the structure did not collapse, do record accurately the
412 emplacement temperatures with very small departures from the initial values.
413 By contrast, results from configuration B (Fig. 6f) indicate that the mixing between a
414 collapsed wall and the PDC deposit promotes a very fast and efficient heat transfer due to
415 the enhanced contact surface available.
416
417 INSERT FIG. 6 HERE
418
419 Fig. 6f shows that the initial thermal disequilibrium, though highly simplified geometrically,
420 rapidly smooths, with a T drop of more than 100°C inside the PDC deposit domains

421 achieved in the first 3 hours of simulation. Six hours are sufficient to homogenise the
422 temperature in the whole computational domain at an average value of less than 200°C,
423 more than 150°C lower than the initial PDC temperature. At the same time, once re-
424 equilibrated, the temperatures in the collapsed domain remain almost constant to the end
425 of the simulation after 24 hours. Supplementary runs performed for configuration B with a
426 finer cell-grid of 0.5 cm in a 30 cm x 30 cm domain (Appendix 3) indicate that the thermal
427 equilibration occurs within the first 15 minutes. These results explain the relatively similar
428 and low T recorded by both lithic and charcoal at sites VP3 and VP4, i.e. where the PDC
429 deposits are fully mixed with portion of collapsed walls of the Villa.
430
431 **6. Discussion**
432
433 What we know about thermal processes within PDCs and their deposits is still rather
434 vague. Current knowledge relies on a very limited number of direct measurements of
435 deposit temperatures taken with thermocouples from the shallowest part of deposits when
436 and where approachable, and a number of studies of the TRM of embedded lithic clasts
437 and reflectance of charcoal (Table S1, in Appendix 1). Some of the main still open
438 questions are: i) what is the actual relationship between the temperature of the PDC
439 deposit and the temperature of the parent current; ii) what temperature is actually recorded
440 by commonly used deposit proxies, considering (a) the inherent thermal disequilibrium of
441 the poly-dispersed and poly-component pyroclastic material, (b) the local interaction with
442 the environment, and (c) the density and thermal stratification within PDCs.
443 Data from the Villa dei Papiri show that temperatures retrieved from TRM of lithic clasts
444 are in excellent agreement with temperatures derived from the reflectance of charcoal
445 fragments taken at the very same sites by Caricchi et al. (2014) (Table 1, Fig. 5). This
446 agreement indicates that temperatures in the deposit at each site remained stable for time-

447 scales comparable with the acquisition times for both proxies, i.e. for at least 24 hours.
448 These results are also in good agreement with numerical simulations, which show, within
449 24 hours, a substantial stability of the temperature close to initial values even very close to
450 a cold substrate, which in our case is the wall of the Villa (Fig. 6c). This is due to the low
451 thermal conductivity of glass shards and crystals that form the ash matrix, so that, in
452 absence of convective effects promoted for example by water vapourisation or other kinds
453 of physical mixing with cold materials (e.g. collapsed walls), the timescale of deposit
454 cooling is much longer than that required for equilibration of lithics and charcoal fragments.
455 This suggests that the values retrieved from our proxies record the deposit temperature
456 very close to that of emplacement. Our data therefore indicate that, in the case of Villa dei
457 Papiri, the highest measured temperatures away from areas of obvious mixing of the
458 deposit with either water (e.g. VP8) or collapsed walls (e.g. VP3, VP4) represent not only
459 the deposit temperatures but are very close to the PDC emplacement temperatures. We
460 also notice that lava lithic clasts sampled for our TRM analyses have been taken from
461 massive lapilli tuff facies, where the ash fraction, both coarse and fine, represents between
462 50 and 90%wt of the deposit, with most common values >75%wt (Gurioli et al., 2002;
463 Appendix 2). Available literature indicates that particles in the ash fraction equilibrate
464 almost instantaneously with the ambient (e.g. Wilson et al., 1978; Thomas and Sparks,
465 1992). The ash fraction can therefore be assumed as continuously thermally equilibrated
466 within flow and at deposition. Possible sources of thermal inhomogeneity (both as heat
467 sources or heat sinks) in the deposit could therefore be related to the presence of large
468 lapilli or bomb sized clasts. Bomb sized clasts in the primary AD79 deposits at Villa dei
469 Papiri are very rare and lapilli represent usually less than 10-15%wt of the deposit. These
470 proportions already suggest that the largest contribution to the deposit temperature is
471 provided by the ash fraction inside which the lithics (and the charcoal measured in Caricchi
472 et al., 2014) had been sampled. The deposit temperatures retrieved from sites with no

visible convective interaction with either water or collapsed walls, though variable, all sit at the high-end of the thermal spectrum of the deposits (> 300 °C) and strongly suggest a common origin, which we interpret as provided by the ash matrix. If that is true, as we believe our data clearly indicate, then the measured deposit temperature not only is very close to the emplacement temperature, but also to the temperature of the basal and more concentrated part of the flow close to the depositional boundary layer (*sensu* Branney and Kokelaar, 2002; see also Benage et al., 2016) (Fig. 7). We therefore conclude that, close to their flow boundary layer, incoming PDCs at Herculaneum had a bulk temperature > 300 °C, most likely around 350 °C (based on the most frequent values retrieved; Fig. 5), carried essentially by the most abundant ash fraction. This conclusion is very important as it answers a long-standing debate on the actual significance of the deposit temperature in respect to the parent flow. Some authors had, in fact, questioned the possibility to transfer directly deposit temperatures into flow temperatures (e.g. Bardot, 2000; Cioni et al., 2004; Sulpizio et al., 2008; Zanella et al., 2007). We suggest here that the emplacement temperature of ash-matrix supported PDC deposits essentially reflects that of the parent flow (Fig. 7), as conductive cooling of the deposit is much slower than the acquisition time for commonly used proxies, namely lithic clasts and charcoal.

Based on the above considerations we propose a detailed reconstruction of the destruction and burial of the Villa dei Papiri from the PDCs that stroke Herculaneum during the evening and night between the 24 and the 25 of August AD79 (Fig. 8).

The first PDC that reached the Villa was EU2/3pf, i.e. the PDC that formed at the transition between the two main sustained plinian phases EU2 and EU3 both SE-ward directed and therefore not recorded at Herculaneum (Fig. 8a,c; Gurioli et al., 2002). The PDC was able to unroof the Villa and partially destroy sections of it, but most of the main structure remained in place. Debris mixed within EU2/3pf deposits at site VP4 relate to such event (Fig. 8b). At the same time the PDC crossed the coastline just in front of the Villa, entered

499 the sea depositing and pushing forward the sea-shore (Fig. 8b). Deposit temperatures are
500 highly inhomogeneous (Table 1), with the lowest measured in this study (180-200°C) and
501 reflect rapid post-emplacement heat transfer processes of mixing with sea-water/vapour
502 and debris. Timescales of such processes are < 1 hour, i.e. the time-scale needed for 1-3
503 cm sized lithics to equilibrate with the embedding deposits (Cioni et al., 2004). After a short
504 pause associated with the restoration of the EU3 buoyant plume which kept depositing
505 pumice fallout to the SE of the volcano (Fig. 8c), a second major PDC (EU3pf) reached the
506 Villa dei Papiri site, partly burying the still standing main edifice (Fig. 8d). EU3pf however
507 did not cause major collapses to the structure, nor it interacted with the sea-water,
508 previously buried by the EU2/3pf deposits. Deposit temperatures in EU3pf average at
509 around 350°C (Table 1 and Fig. 5) even within or very close to the Villa (VP1, VP2), both
510 from TRM data presented herein and from charcoal data presented by Caricchi et al.
511 (2014) and reflect the average temperature of the parent PDC close to its depositional
512 boundary layer (Fig. 7). The following PDC, EU4pf, reached the Villa after the transition
513 from the buoyant EU3 phase and the beginning of the caldera collapse phase which was
514 thereon dominated by PDCs (Fig. 8e,f). With the arrival of the EU4 PDC, the Villa was
515 completely buried and the deposits locally mixed with debris from the collapsed walls of
516 the summit floor, by then totally unroofed (Fig. 8g). Based on the highest temperatures
517 retrieved in EU4 we interpret the parent PDC to have arrived in town with a temperature
518 just above 350°C close to its depositional boundary layer, which is similar to that of the
519 previous EU3pf.
520
521 INSERT FIG. 7 AND FIG. 8 HERE
522
523 The results of our study may help in understanding of the outstanding degree of
524 preservation of the objects found inside the Villa dei Papiri. This edifice is very famous in
525 the archaeological literature for having well preserved wooden objects (Guidoboni et al.,

2009) and very rare documents as delicate as papyri rolls (Mocella et al., 2015). These findings are unique and we argue that the style of thermal interaction between the PDC deposits and the edifice controls the degree of preservation of the objects. On the one side, rooms poorly- or un-invaded by the PDC deposits may have experienced a rather slow heating through the intact walls, allowing for efficient dehydration of the wooden materials without burning. On the other side, where collapses of the walls occurred, the average temperature quickly dropped at or below 200°C, limiting the effects of charcoalification. We conclude that the Villa dei Papiri owes its fame to the history of its burial and thermal exchange with the AD79 PDC deposits.

A broader implication of our study is that local interactions may change substantially the thermal dynamics of the flow and of the related deposits, affecting not only the impact on infrastructures but the potential for human survival during PDC events, as witnessed for example during the Merapi 2010 eruption (Baxter et al., 2017).

7. Conclusions

We have presented a detailed study of the temperature of the AD79 PDC deposits that progressively destroyed and buried a large ancient Roman edifice, the Villa dei Papiri, at Herculaneum. We measured the TRM of lithic clasts embedded in the ash matrix of massive and chaotic facies and compared the results with temperatures retrieved from the reflectance of charcoal fragments collected at the very same sites by Caricchi et al. (2014). The excellent overlap between the two datasets allows to draw several important conclusions very relevant for our conceptual and physical understanding of pyroclastic density currents, as well as to reconstruct in detail the history of the thermal interaction between the incoming PDCs and the Villa dei Papiri edifice and its environment.

The main conclusions are:

1) The temperature of the ash-matrix supported, massive and chaotic PDC deposits

552 remains stable over time-scales of 24 hours that encompass the different acquisition times
553 for both TRM and charcoal proxies; this temperature stability suggests that the
554 emplacement temperature of the ash-matrix, where unaffected by external factors (see
555 point 2 below), cannot be substantially different from that of the deposit at the time of
556 acquisition; in turn, the temperature of the basal part of the current, close to its
557 depositional boundary layer prior to deposition, cannot be substantially different. We
558 conclude that the deposit temperature is an excellent proxy for the temperature of the base
559 of PDCs. This conclusion underlines the importance of studies on the emplacement
560 temperatures of PDC deposits to understand their flow dynamics (e.g. Benage et al.,
561 2016).
562 2) The temperature of PDC deposits is significantly and quickly affected by external factors
563 across the acquisition times of TRM and charcoal proxies only where convective mixing
564 occurs, either with external water, rock debris or else; such occurrences define local
565 thermal domains within the PDC deposits and their thermal disequilibrium with the
566 surroundings can be maintained for time-scales much longer than 24 hours. This
567 conclusion is important as future work must take into account local thermal
568 inhomogeneities of the PDC deposits.
569 3) The reconstruction of the thermal interactions at Villa dei Papiri shows that the first
570 incoming PDC had the largest degree of mixing with both debris from the unroofing of the
571 edifice and partial collapses, along with the interaction with the sea facing the Villa; the
572 following PDCs were thermally affected by the Villa only where collapses occurred,
573 otherwise the purely conductive thermal equilibration along standing walls takes much
574 longer than 24 hours even at <50 cm from contact between PDC deposit and wall.
575 We argue that the varying style of thermal interactions between PDC deposits and the
576 edifice largely controlled the state of preservation of the archeological findings at Villa dei
577 Papiri. This conclusion may bear significant implications for interpreting the highly variable

state of preservation of archeological remains covered by hot pyroclastic deposits, in the Neapolitan region and elsewhere.

Acknowledgements

This work was funded by the DPC-INGV grant Project V1 – UR RM3 (resp. C. Romano).

Figure captions

Figure 1: a) Location of Villa dei Papiri and Herculaneum respect to Vesuvius; b) detailed map of the Villa dei Papiri excavations and location of sampling sites; c,d) volcano-ward and sea-ward views of the Villa dei Papiri archeological excavation and location of sampling sites (VP) in relation with the stratigraphy of the AD79 eruption. Temperature ranges in blue indicate results from TRM of lithic clasts obtained in this study, compared with values obtained from charcoal by Caricchi et al. (2014) indicated in red. White numbers indicate elevations in m a.s.l. (photo and elevation survey courtesy of Superintendence for Archaeology of Herculaneum).

Figure 2: Examples of the demagnetization results on Zijderveld diagrams: solid/open dots represent declination/apparent inclination. Red/blue lines are the interpolated high-T and low-T magnetization components, respectively. Examples are selected from each sampled site.

Figure 3: Example of procedure for determination of the deposition temperature interval at site VP6; a) the T_{dep} is estimated from the overlapping T_r ranges for all lithic clasts sampled at this site; b) Frequency-histogram of temperatures showing the gaussian distribution of

obtained values. Note that for each T interval we count the number of clasts that are fully included in the interval considered, plus all those that touch the extreme of the values of the bin.

Table 1: Site deposition temperature, T_{dep} (°C). Legend: n/N number of T_r interval in the overlapping range out of number of measured lithic clasts; type A, B, C, D as in Cioni et al. (2004). The question mark indicates the poorly constrained Zjiderveld diagrams. $T_{charcoal}$ indicates temperatures retrieved by Caricchi et al. (2014) from the analysis of the reflectance of charcoal fragments sampled at the very same sites.

Figure 4: a) plan view of sampling sites (see also Fig. 1); b) detail of the large gas pipe affecting EU2/3; c) basement floor of the Villa where the EU2/3 ignimbrite is both mixed with collapsed debris and affected by sea-water mixing; d) third floor of the Villa where the EU4 ignimbrite is partly mixed with collapsed debris; data in red (and in (c)) are from Caricchi et al. (2014).

Figure 5: Deposit temperature at each measured site (see Fig. 1 for location). Open circles indicate the mean values for TRM samples and bars the related T interval; Red bars indicate temperatures retrieved from charcoal reflectance from Caricchi et al (2014). The averages of undisturbed and mixed facies are given by dashed lines.

Table 2: Physical properties of rocks used for the simulation in Heat3D (see text for explanation).

Figure 6: Main results of the Heat3D numerical modeling of heat transfer between the ignimbrite (red domain) and the wall (blue domain) for the two chosen configurations at

t=0: A is the intact wall; B is the collapsed wall mixed with the ignimbrite; the cell-grid is 5 cm. Diagrams below each initial configuration show the temperature evolution over 24 hours taken along the green line.

Figure 7: Cartoon illustrating the different thermal interactions of the incoming PDC with the environment, which promote rapid changes of temperature of the deposit in different though very close settings. Note that temperature at the base of the incoming PDC is everywhere ~350°C, similar to that of the deposit unless mixing with either debris or water occurs during emplacement.

Figure 8: Reconstruction of the progressive destruction and burial of the Villa dei Papiri; stratigraphic units according to Gurioli et al. (2002); chronology according to Sigurdsson et al (1982). See text for explanation.

References

Barberi, F., Cioni, R., Rosi, M., Santacroce, R., Sbrana, A., Vecci, R., 1989. Magmatic and phreatomagmatic phases in explosive eruptions of Vesuvius as deduced by grain-size and component analysis of the pyroclastic deposits. J. Volcanol. Geotherm. Res. 38, 287–307. doi:10.1016/0377-0273(89)90044-9

Bardot, L., 2000. Emplacement temperature determinations of proximal pyroclastic deposits on Santorini, Greece, and their implications. Bull. Volcanol. 61, 450–467. doi:10.1007/PL00008911

Baxter, P. J., Jenkins, S., Seswandhana, R., Komorowski, J. C., Dunn, K., Purser, D., Voight. B. & Shelley, I. (2017). Human survival in volcanic eruptions: thermal injuries

656 in pyroclastic surges, their causes, prognosis and emergency
657 management. Burns, 43(5), 1051-1069.
658 Benage, M. C., Dufek, J., & Mothes, P. A. (2016). Quantifying entrainment in pyroclastic
659 density currents from the Tungurahua eruption, Ecuador: Integrating field proxies with
660 numerical simulations. Geophysical Research Letters, 43(13), 6932-6941.
661 Branney, M. J., & Kokelaar, B. P. (2002). Pyroclastic density currents and the
662 sedimentation of ignimbrites. Geological Society of London. Special Publication.
663 Carey, S., Sigurdsson, H., 1987. Temporal variations in column height and magma
664 discharge rate during the 79 A.D. eruption of Vesuvius. Geol. Soc. Am. Bull. 99, 303–
665 314. doi:10.1130/0016-7606(1987)99<303
666 Caricchi, C., Vona, A., Corrado, S., Giordano, G., Romano, C., 2014. AD79 Vesuvius PDC
667 deposits' temperatures inferred from optical analysis on woods charred in-situ in the
668 Villa dei Papiri at Herculaneum (Italy). J. Volcanol. Geotherm. Res. 289, 14–25.
669 doi:10.1016/j.jvolgeores.2014.10.016
670 Cioni, R., Marianelli, P., Sbrana, A., 1992. Dynamics of the A.D. 79 eruption: stratigraphic,
671 sedimentological and geochemical data on the successions from the Somma-
672 Vesuvius southern and eastern sectors. Acta Vulcanol. 2, 109–123.
673 Cioni, R., Gurioli, L., Lanza, R., Zanella, E., 2004. Temperatures of the A.D. 79 pyroclastic
674 density current deposits (Vesuvius, Italy). J. Geophys. Res. 109, B02207.
675 doi:10.1029/2002JB002251
676 Dioguardi, F., & Dellino, P. (2014). PYFLOW: A computer code for the calculation of the
677 impact parameters of Dilute Pyroclastic Density Currents (DPDC) based on field
678 data. Computers & Geosciences, *66*, 200-210.
679 Doronzo, D. M., Martí, J., Dellino, P., Giordano, G., & Sulpizio, R. (2016). Dust storms,
680 volcanic ash hurricanes, and turbidity currents: physical similarities and differences
681 with emphasis on flow temperature. Arabian Journal of Geosciences, 9(4), 290.

Formatted: English (United States)

682 Eychenne, J., Pennec, J.-L., Troncoso, L., Gouhier, M., Nedelec, J.-M., 2012. Causes and
683 consequences of bimodal grain-size distribution of tephra fall deposited during the
684 August 2006 Tungurahua eruption (Ecuador). Bull. Volcanol. 74, 187–205.
685 doi:10.1007/s00445-011-0517-5
686 Eppelbaum, L., Kutasov, I., & Pilchin, A. (2014). Thermal properties of rocks and density of
687 fluids. In Applied geothermics (pp. 99-149). Springer Berlin Heidelberg.
688 Giordano, G., & Doronzo, D. M. (2017). Sedimentation and mobility of PDCs: a reappraisal
689 of ignimbrites' aspect ratio. Sci. Rep., *7*, 4444.
690 Guidobaldi, M.P., Esposito, D., Formisano, E., 2009. L'insula I, l'insula nord occidentale e
691 la villa dei Papiri di Ercolano: una sintesi delle conoscenze alla luce delle recenti
692 indagini archeologiche. In: Serra, Fabrizio (Ed.), Vesuviana Vol.1, 43–180.
693 Gurioli, L., Cioni, R., Sbrana, A., Zanella, E., 2002. Transport and deposition of pyroclastic
694 density currents over an inhabited area: the deposits of the AD 79 eruption of
695 Vesuvius at Herculaneum, Italy. Sedimentology 49, 929–953.
696 Gurioli, L., Houghton, B.F., Cashman, K. V, Cioni, R., 2005. Complex changes in eruption
697 dynamics during the AD79 eruption of Vesuvius. Bull. Volcanol. 67, 144–159.
698 doi:10.1007/s00445-004-0368-4
699 Gurioli, L., Zanella, E., Pareschi, M.T., Lanza, R., 2007. Influences of urban fabric on
700 pyroclastic density currents at Pompeii (Italy): 1. Flow direction and deposition. J.
701 Geophys. Res. 112, B05213. doi:10.1029/2006JB004444
702 Jenkins, S., Komorowski, J.C., Baxter, P.J., Spence, R., Picquout, A., Lavigne, F., Surono,
703 2013. The Merapi 2010 eruption: An interdisciplinary impact assessment
704 methodology for studying pyroclastic density current dynamics. J. Volcanol.
705 Geotherm. Res. 261, 316–329. doi:10.1016/j.jvolgeores.2013.02.012
706 Kent, D. V, Ninkovich, D., Pescatore, T., Sparks, R.S.J., 1981. Palaeomagnetic
707 determination of emplacement temperature of Vesuvius AD 79 pyroclastic deposits.

Formatted: Italian (Italy)

Nature 290, 393–396.

Lange, R. A., & Carmichael, I. S. (1987). Densities of Na2O-K2O-CaO-MgO-FeO-Fe2O3-Al2O3-TiO2-SiO2 liquids: new measurements and derived partial molar properties. Geochimica et Cosmochimica Acta, 51(11), 2931-2946.

Lavallée, Y., Wadsworth, F.B., Vasseur, J., Russell, J.K., Andrews, G.D.M., Hess, K.-U., von Aulock, F.W., Kendrick, J.E., Tuffen, H., Biggin, A.J., Dingwell, D.B., 2015. Eruption and emplacement timescales of ignimbrite super-eruptions from thermo-kinetics of glass shards. Front. Earth Sci. 3, 1–11. doi:10.3389/feart.2015.00002

Lesti, C., Porreca, M., Giordano, G., Mattei, M., Cas, R.A.F., Wright, H.M.N., Folkes, C.B., Viramonte, J., 2011. High-temperature emplacement of the Cerro Galán and Toconquis Group ignimbrites (Puna plateau, NW Argentina) determined by TRM analyses. Bull. Volcanol. 73, 1535–1565. doi:10.1007/s00445-011-0536-2

Lirer, L., Pescatore, T., Booth, B., Walker, G.P.L., 1973. Two plinian pumice-fall deposits from Somma-Vesuvius, Italy. Geol. Soc. Am. Bull. 84, 759–772.

Mastrolorenzo, G., Petrone, P.P., Pagano, M., Incoronato, A., Baxter, P.J., Canzanella, A., Fattore, L., 2001. Herculaneum victims of Vesuvius in ad 79. Nature 410, 769–70. doi:10.1038/35071167

McClelland, E.A., Druitt, T.H., 1989. Palaeomagnetic estimates of emplacement temperatures of pyroclastic deposits on Santorini, Greece. Bull. Volcanol. 51, 16–27.

Mocella, V., Brun, E., Ferrero, C., & Delattre, D. (2015). Revealing letters in rolled Herculaneum papyri by X-ray phase-contrast imaging. Nat. Comm., 6, 5895.

Paterson, G.A., Roberts, A.P., Mac Niocaill, C., Muxworthy, A.R., Gurioli, L., Viramonté, J.G., Navarro, C., Weider, S., 2010. Paleomagnetic determination of emplacement temperatures of pyroclastic deposits: an under-utilized tool. Bull. Volcanol. 72, 309–330. doi:10.1007/s00445-009-0324-4

Pensa, A., Porreca, M., Corrado, S., Giordano, G., Cas, R., 2015a. Calibrating the pTRM

Formatted: English (United States)

Formatted: English (United States)

734 and charcoal reflectance (Ro%) methods to determine the emplacement temperature
735 of ignimbrites: Fogo A sequence, S??o Miguel, Azores, Portugal, as a case study.
736 Bull. Volcanol. 77. doi:10.1007/s00445-015-0904-4
737 Pensa, A., Giordano, G., Cas, R.A.F., Porreca, M., 2015b. Thermal state and implications
738 for eruptive styles of the intra-Plinian and climactic ignimbrites of the 4.6 ka Fogo A
739 eruption sequence, São Miguel, Azores. Bull. Volcanol. 77, 99. doi:10.1007/s00445-
740 015-0983-2
741 Porreca, M., 2004. Applicazioni di metodi paleomagnetici per lo studio della messa in
742 posto di flussi piroclastici. Il caso delle unita` vulcaniche recenti del cratere di Albano
743 (Italia Centrale), Ph.D. thesis, 118 pp., Univ. of Roma Tre, Rome.
744 Porreca, M., Giordano, G., Mattei, M., & Musacchio, P. (2006). Evidence of two Holocene
745 phreatomagmatic eruptions at Stromboli volcano (Aeolian Islands) from
746 paleomagnetic data. Geophy. Res. Lett., 33(21).
747 Porreca, M., Cifelli, F., Soriano, C., Giordano, G., Romano, C., Conticelli, S., & Mattei, M.
748 (2014). Hyaloclastite fragmentation below the glass transition: An example from El
749 Barronal submarine volcanic complex (Spain). Geology, *42*(1), 87-90.
750 Robertson, E. C. (1988). Thermal properties of rocks. US Geological Survey, Open-File
751 Report No. 88-441.
752 Scott, A.C., Glasspool, I.J., 2005. Charcoal reflectance as a proxy for the emplacement
753 temperature of pyroclastic flow deposits. Geology 33, 589–592.
754 doi:10.1130/G21474.1
755 Sigurdsson, H., Cashdollar, S., Sparks, R.S.J., 1982. The Eruption of Vesuvius in A. D. 79:
756 Reconstruction from Historical and Volcanological Evidence. Am. J. Archaeol. 86, 39–
757 51.
758 Sigurdsson, H., Carey, S., Cornell, W., Pescatore, T., 1985. The eruption of Vesuvius in
759 A.D. 79. National Geographic Research 1, 332–387.

760 Sulpizio, R., Zanella, E., Macías, J.L., 2008. Deposition temperature of some PDC
761 deposits from the 1982 eruption of El Chichon volcano (Chiapas, Mexico) inferred
762 from rock-magnetic data. J. Volcanol. Geotherm. Res. 175, 494–500.Sulpizio, R.,
763 Zanella, E., Macías, J. L., & Saucedo, R. (2015). Deposit temperature of pyroclastic
764 density currents emplaced during the El Chichón 1982 and Colima 1913
765 eruptions. *Geological Society, London, Special Publications*, *396*(1), 35-49.
766 Tema. E., Zanella, E., Pavon-Carrasco, F.J., Kondopoulou, D., Pavlides, S., 2015.
767 Palaeomagnetic analysis on pottery as indicator of the pyroclastic flow deposits
768 temperature: new data and statistical interpretation from the Minoan eruption of
769 Santorini, Greece. Geophys. J. Int. 203, 33-47.
770 Thomas, R.M.E., Sparks, R.S.J., 1992. Cooling of tephra during fallout from eruption
771 columns. Bull. Volcanol. 54, 542–553.
772 Trolese, M., Giordano, G., Cifelli, F., Winkler, A., & Mattei, M. (2017). Forced transport of
773 thermal energy in magmatic and phreatomagmatic large volume ignimbrites:
774 Paleomagnetic evidence from the Colli Albani volcano, Italy. Earth Planet. Sci.
775 Lett., *478*, 179-191.
776 Turcotte, D. L., & Schubert, G. (2014). *Geodynamics*. Cambridge University Press.
777 Willcock, M. A. W., Cas, R. A. F., Giordano, G., & Morelli, C. (2013). The eruption,
778 pyroclastic flow behaviour, and caldera in-filling processes of the extremely large
779 volume (> 1290km 3), intra-to extra-caldera, Permian Ora (ignimbrite) Formation,
780 southern Alps, Italy. J. Volcanol. Geotherm. Res., *265*, 102-126.
781 Wilson, L., Sparks, R.S.J., Huang, T.C., Watkins, N.D., 1978. The Control of Volcanic
782 Column Heights by Eruption Energetics and Dynamics. J. Geophys. Res. 83, B4.
783 Whittington, A.G., Hofmeister, A.M., Nabelek, P.I., 2009. Temperature-dependent thermal
784 diffusivity of the Earth's crust and implications for magmatism. Nature 458, 319–21.
785 doi:10.1038/nature07818.

Field Code Changed
Formatted: Italian (Italy)
Formatted: English (United States)

786 Wohletz, K., Civetta, L., & Orsi, G. (1999). Thermal evolution of the Phlegraean magmatic
787 system. Journal of Volcanology and Geothermal Research, 91(2-4), 381-414.
788 Wohletz, K., 2008, KWare geological software, 10 July 2008:
789 http://www.ees1.lanl.gov/Wohletz/ Heat.htm (November 2008).
790 Yokoyama, T., Marturano, A., 1997. Volcanic products of the Vesuvius eruption in AD79 at
791 Pompeii, Italy. Opus. Pomp. 1–32.
792 Zanella, E., Gurioli, L., Pareschi, M.T., Lanza, R., 2007. Influences of urban fabric on
793 pyroclastic density currents at Pompeii (Italy): 2. Temperature of the deposits and
794 hazard implications. J. Geophys. Res. 112, B05214. doi:10.1029/2006JB004775
795 Zanella, E., Sulpizio, R., Gurioli, L., Lanza, R., 2015. Temperatures of the pyroclastic
796 density currents deposits emplaced in the last 22 kyr at Somma-Vesuvius (Italy).
797 Geol. Soc. London, Spec. Publ. doi:10.1144/SP396.4
798

Figure 1 LR

Click here to download high resolution image

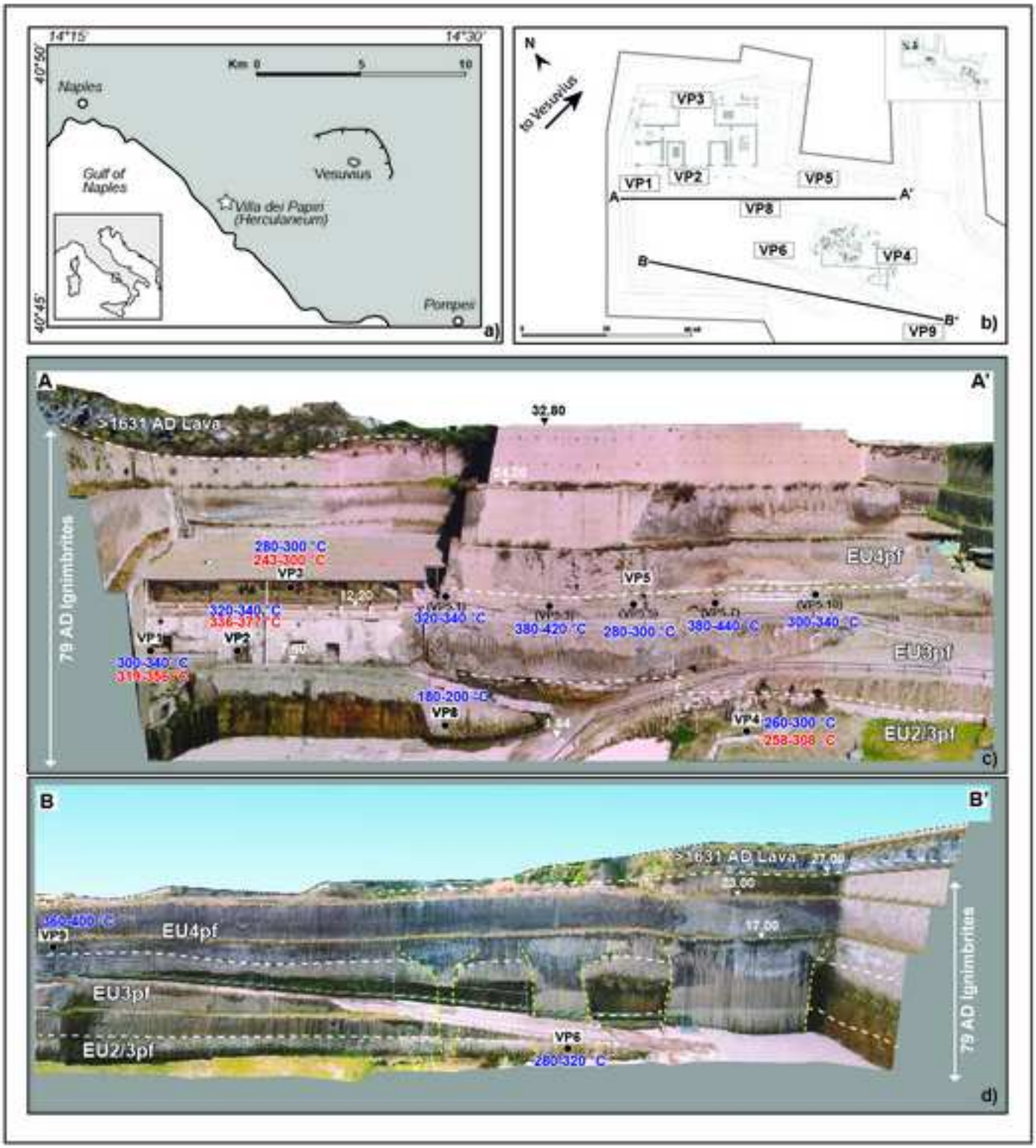

Figure 2

Click here to download Figure: Fig2.pdf

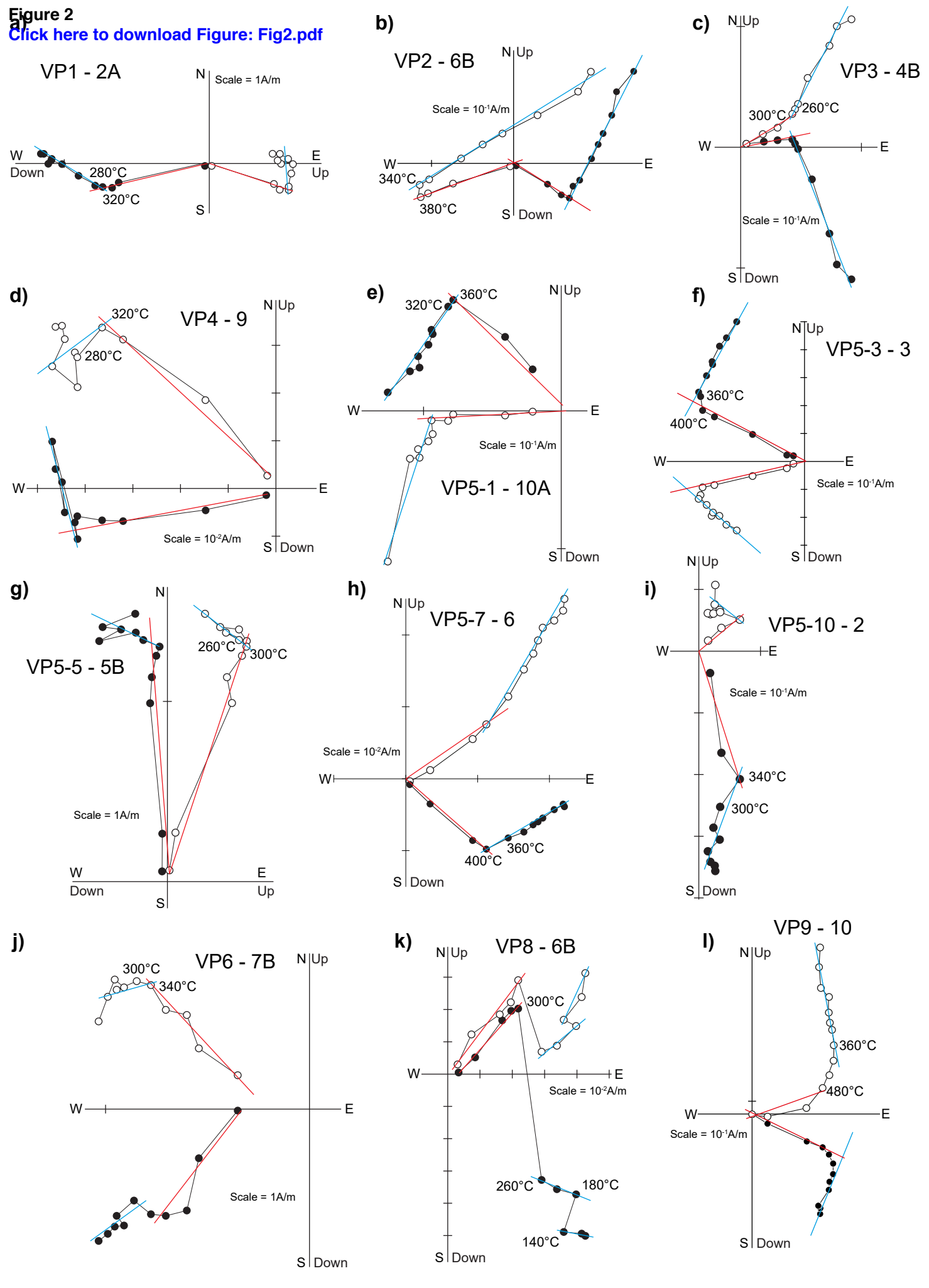

Figure 3

Click here to download Figure: Fig3_V3.pdf

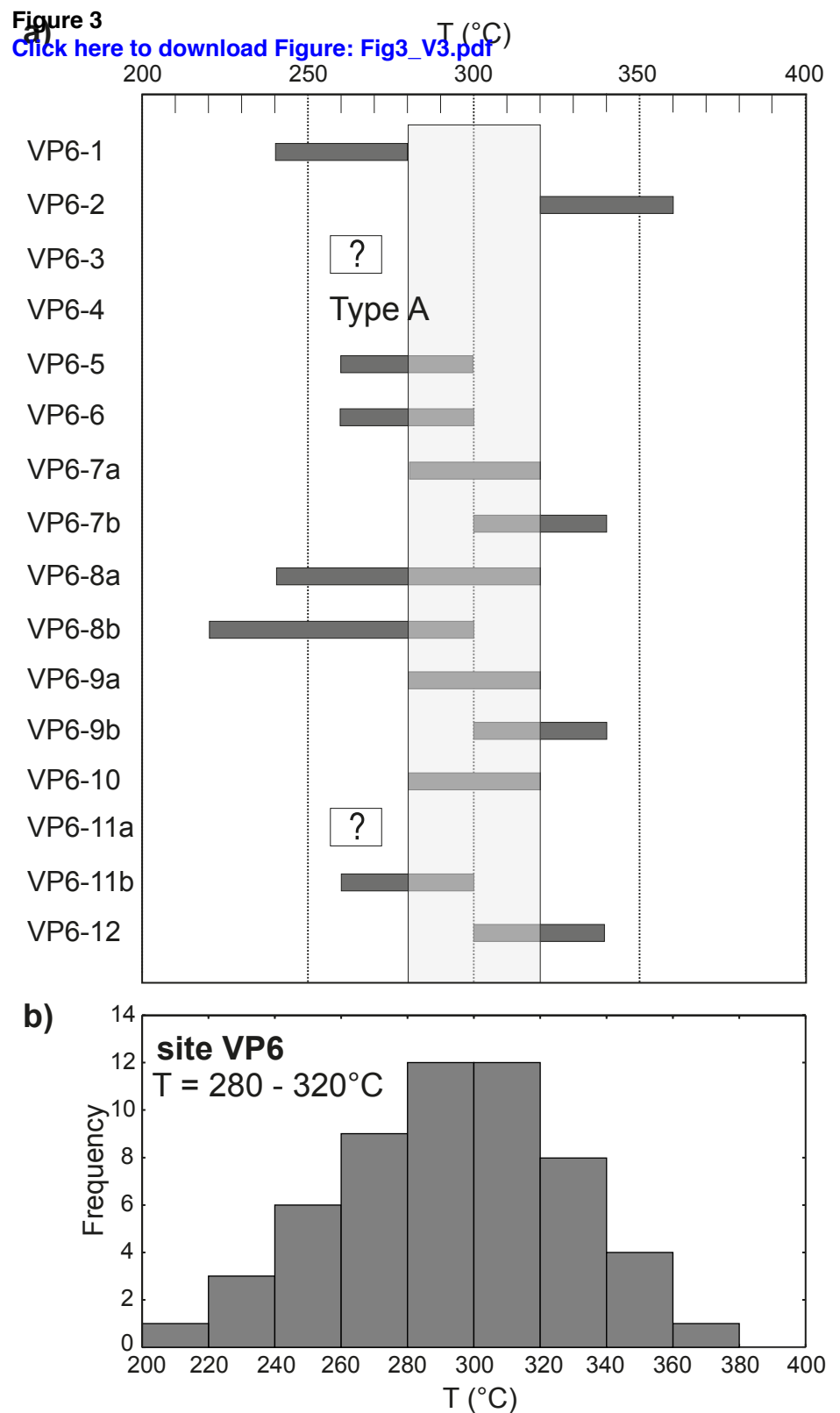

Figure 4 LR

Click here to download high resolution image

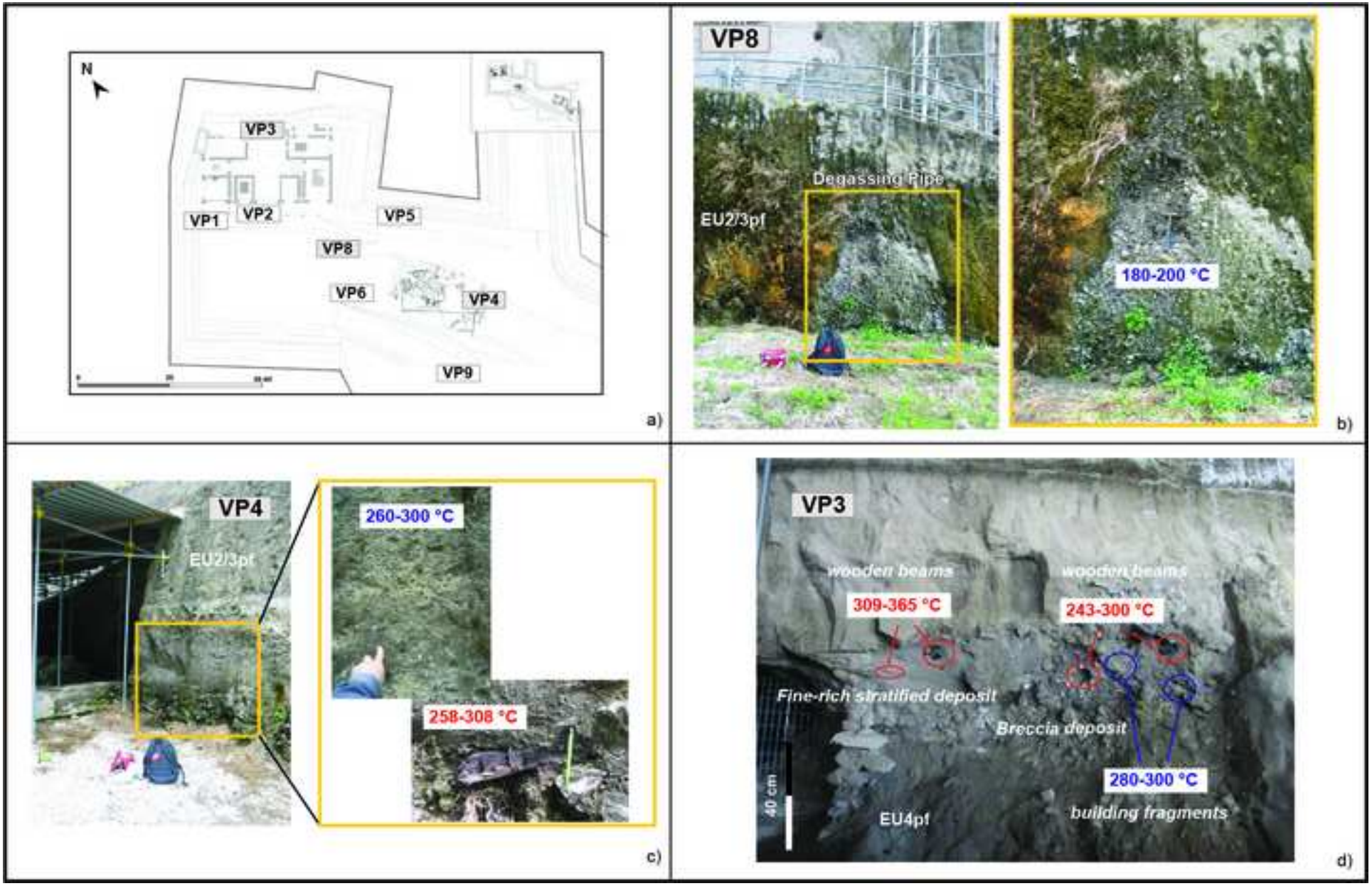

Figure 5

Click here to download Figure: Figure_5_V2.pdf

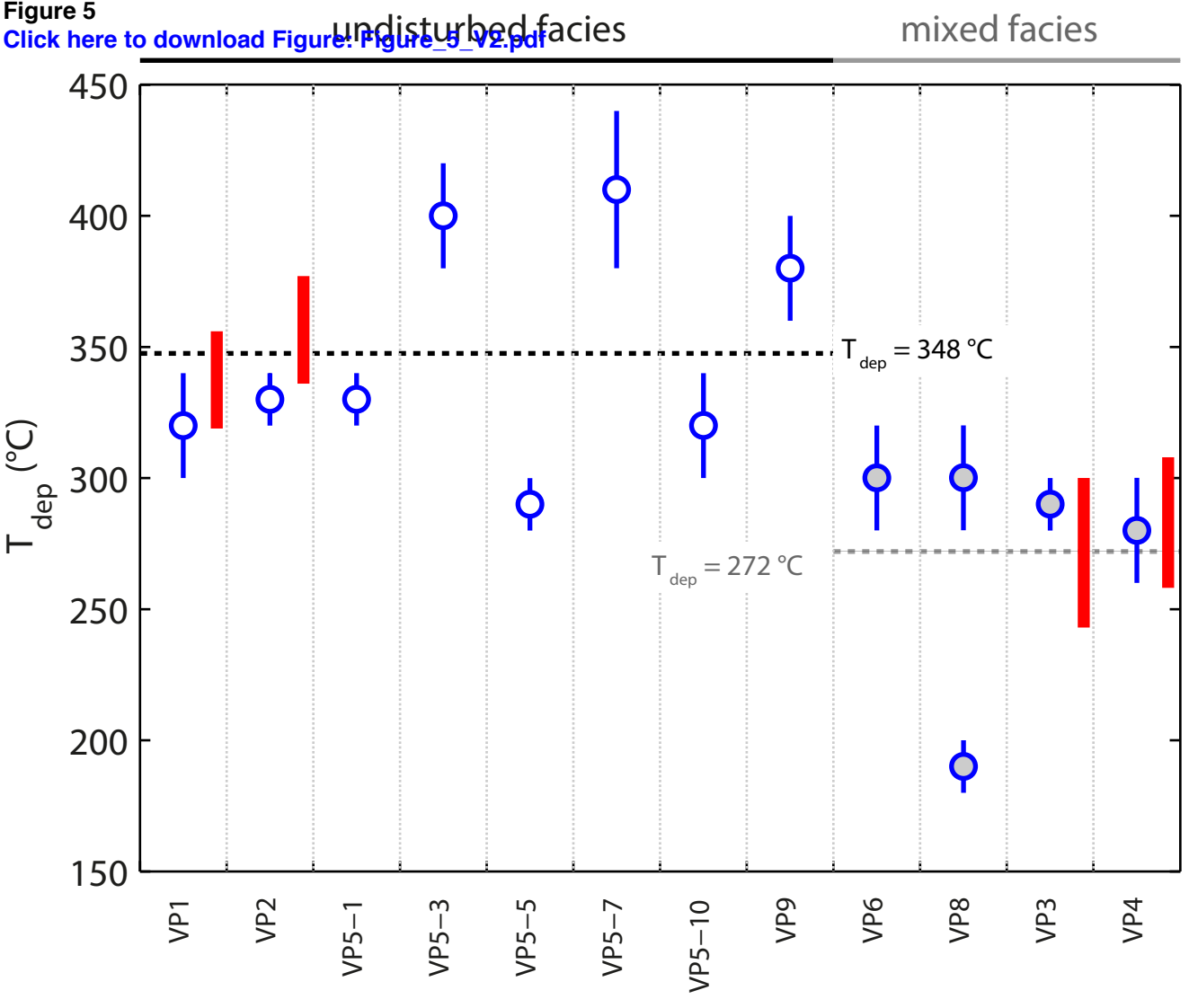

Figure 6 LR

Click here to download high resolution image

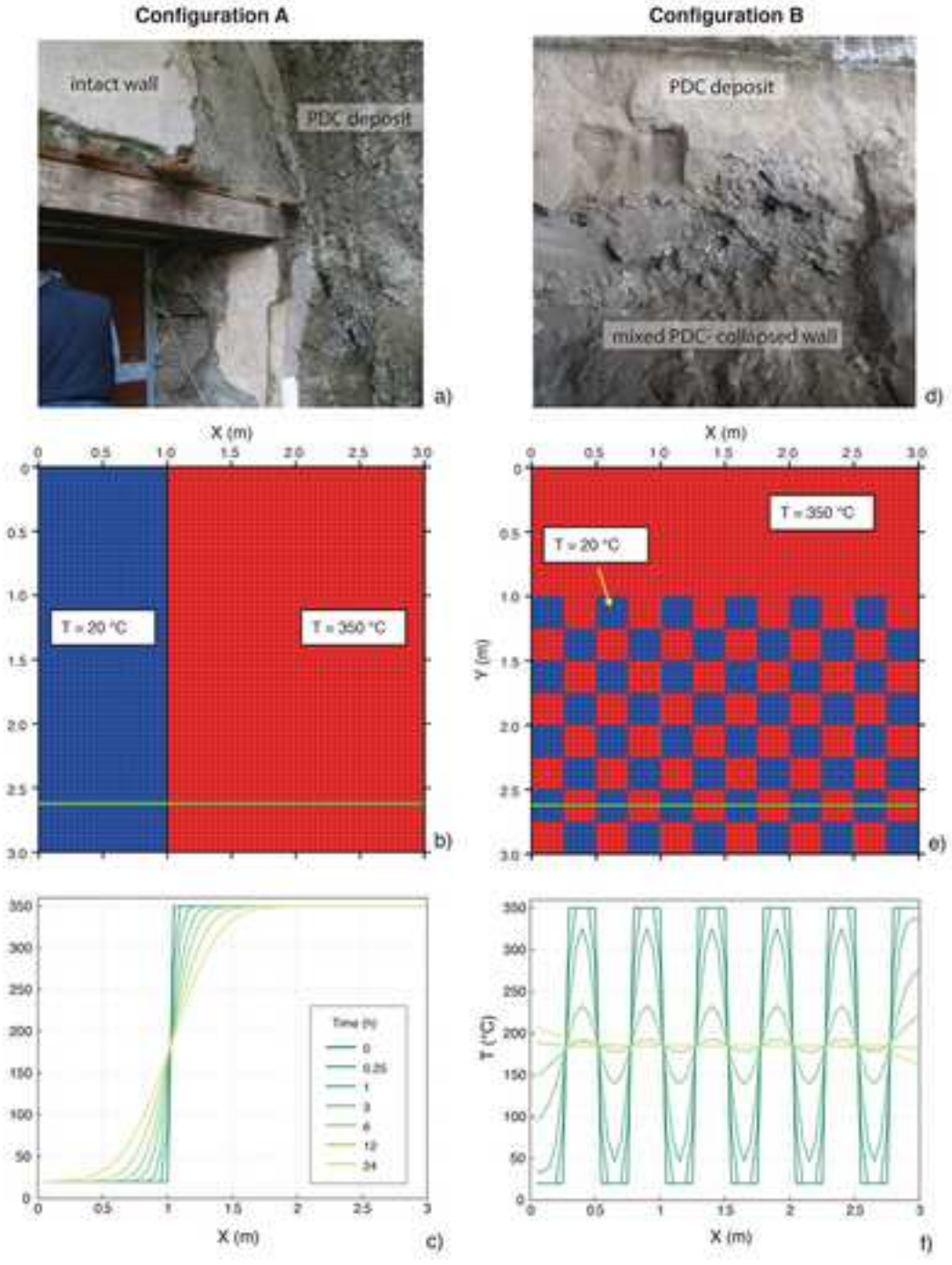

Figure 7

Click here to download Figure: Figure_7.pdf

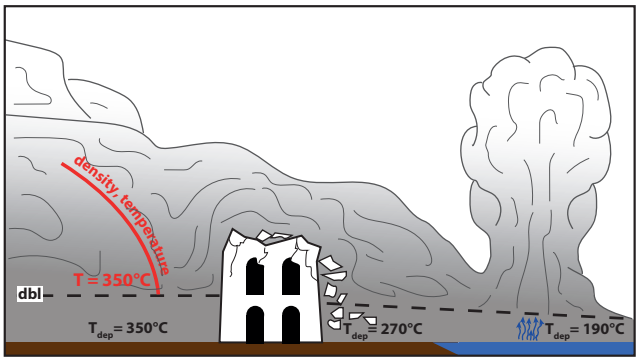

Figure 8 LR

Click here to download high resolution image

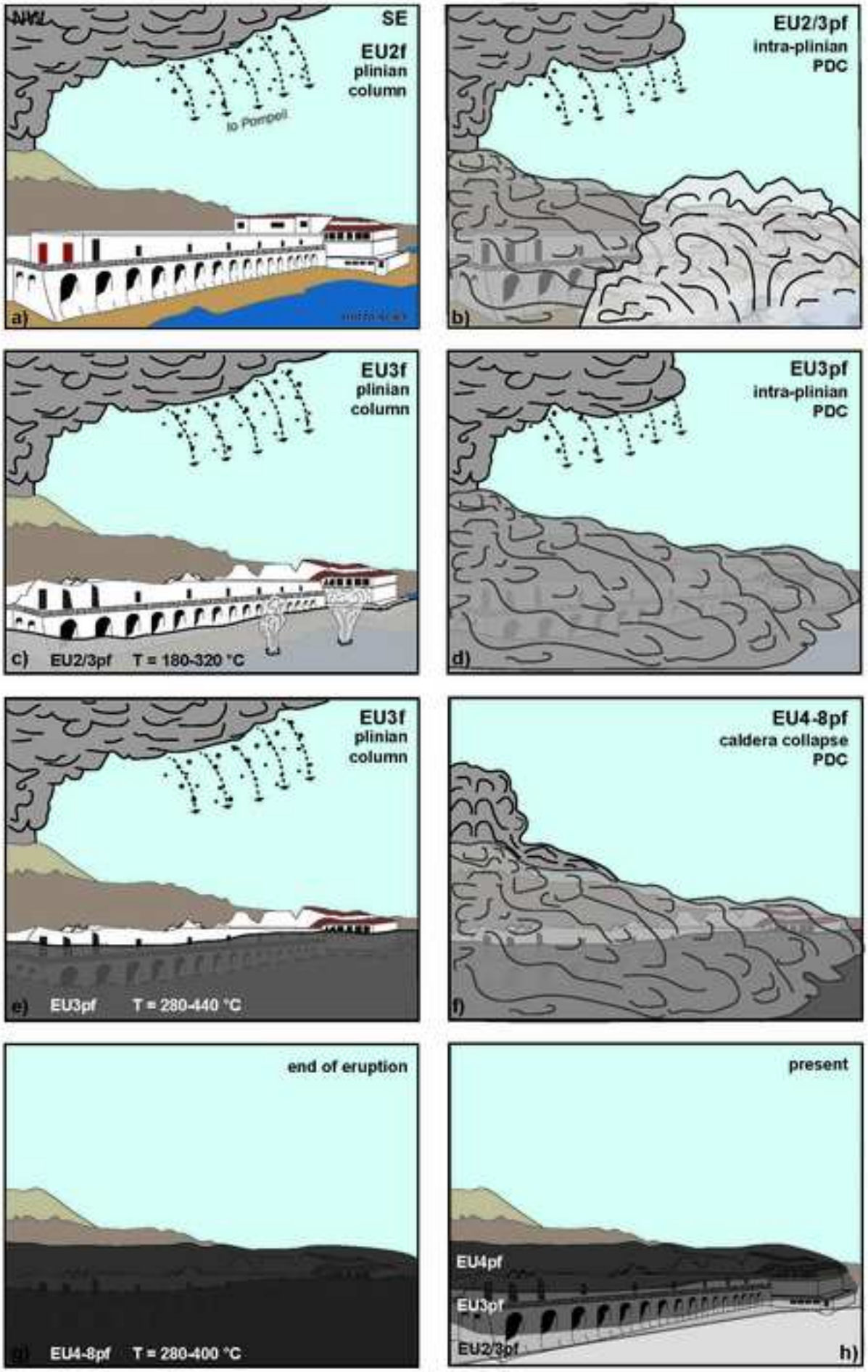

Figure (high-resolution)

Click here to download Figure (high-resolution): Figure_1_HR_2017_12_11.pdf

Figure 4 (high-resolution)

Click here to download Figure (high-resolution): Figure_4_HR_2017_12_12.pdf

Figure 6 (high-resolution)

Click here to download Figure (high-resolution): Figure_6_2017_12_11.pdf

Figure 8 (high-resolution)

Click here to download Figure (high-resolution): Figure_8_HR.pdf

Table 1
Click here to download Table: Table 1.xlsx

Table 1. Results of paleomagnetic analysis.

Eruption Unit[a]	Site	n/N	Type					T_{dep}(°C)	T_{dep}charcoal (°C)[b]	Notes
			A	B	C	D	?			
EU4pf	VP9	3/14	-	-	6	1	7	360-400	-	Unconsolidated lapilli tuff
	VP3	10/12	1	1	7	1	2	280-300	243-300	Mixed debris-lapilli tuff breccia
		-	-	-	-	-	-	-	309-365	Fine-rich stratified deposit
EU3pf	VP5-10	13/16	2	1	9	2	2	300-340	-	Unconsolidated lapilli tuff
	VP5-7	4/11	-	-	2	7	2	380-440	-	Unconsolidated lapilli tuff
	VP5-5	9/16	3	-	9	2	2	280-300	-	Unconsolidated lapilli tuff
	VP5-3	7/13	1	-	7	2	3	380-420	-	Unconsolidated lapilli tuff
	VP5-1	9/16	-	3	10	3	-	320-340	-	Unconsolidated lapilli tuff near undisturbed wall
	VP2	10/16	-	1	14	1	-	320-340	336-377	Unconsolidated lapilli tuff near undisturbed wall
	VP1	9/28	2	--	14	2	10	300-340	319-356	Unconsolidated lapilli tuff near undisturbed wall
EU2/3pf	VP6	13/16	1	-	11	2	2	280-320	-	Zeolitized lapilli tuff
	VP8	10/16	-	-	14	-	2	180-200	-	Lithic rich gas pipe
	VP4	10/16	2	-	9	1	4	260-300	258-308	Mixed debris-lapilli tuff breccia

[a]According to Cioni et al. (2004);[b]T derived from charcolized woods by Caricchi et al. (2014)

Table 2

Click here to download Table: Table 2 physical properties_5 Febbraio 2018.xls

Table 2.

	initial T (°C)	density (kg m^3)	thermal conductivity (W $m^{-1}K^{-1}$)	Specific Heat (J kg^{-1} K^{-1})
ignimbrite	350	1200	0.7	1200
wall	20	2000	1	980

Supplementary material for online publication only

Click here to download Supplementary material for online publication only: Appendix 2.pdf

Supplementary material for online publication only

Click here to download Supplementary material for online publication only: Appendix 1, 3_ 5 febbraio 2008.docx